



# Transient coupled calculations of the Molten Salt Fast Reactor using the Transient Fission Matrix approach



A. Laureau <sup>\*</sup>, D. Heuer, E. Merle-Lucotte, P.R. Rubiolo, M. Allibert, M. Aufiero

*LPSC, Université Grenoble-Alpes, CNRS/IN2P3, 53 rue des Martyrs, F-38026 Grenoble Cedex, France*

## HIGHLIGHTS

- Neutronic ‘Transient Fission Matrix’ approach coupled to the CFD OpenFOAM code.
- Fission Matrix interpolation model for fast spectrum homogeneous reactors.
- Application for coupled calculations of the Molten Salt Fast Reactor.
- Load following, over-cooling and reactivity insertion transient studies.
- Validation of the reactor intrinsic stability for normal and accidental transients.

## ARTICLE INFO

### Article history:

Received 12 March 2016

Received in revised form 18 October 2016

Accepted 18 February 2017

### Keywords:

MSFR  
Transient calculation  
Neutronics  
Thermal hydraulics  
Transient Fission Matrix

## ABSTRACT

In this paper we present transient studies of the Molten Salt Fast Reactor (MSFR). This generation IV reactor is characterized by a liquid fuel circulating in the core cavity, requiring specific simulation tools. An innovative neutronic approach called ‘Transient Fission Matrix’ is used to perform spatial kinetic calculations with a reduced computational cost through a pre-calculation of the Monte Carlo spatial and temporal response of the system. Coupled to this neutronic approach, the Computational Fluid Dynamics code OpenFOAM is used to model the complex flow pattern in the core. An accurate interpolation model developed to take into account the thermal hydraulics feedback on the neutronics including reactivity and neutron flux variation is presented. Finally different transient studies of the reactor in normal and accidental operating conditions are detailed such as reactivity insertion and load following capacities. The results of these studies illustrate the excellent behavior of the MSFR during such transients.

© 2017 Elsevier B.V. All rights reserved.

## 1. Introduction

The reference design of the Molten Salt Fast Reactor (MSFR) is a 3 GWth liquid fuel reactor with a fuel salt volume of 18 m<sup>3</sup> and an average fuel salt temperature of 975 K (Brovchenko et al., 2013; Heuer et al., 2014; Allibert et al., 2016). It comprises three distinct circuits: the fuel circuit, the intermediate circuit and the power conversion system. This paper focuses on the modeling of the fuel circuit in transient calculations. The fuel salt considered is a molten binary fluoride salt with 77.5% of lithium fluoride; the other 22.5% are a mix of heavy nuclei fluorides (thorium and fissile matter). The proportion of fissile matter is adjusted to reach criticality. The circulation period of the fuel salt is around 4 s. As shown in Fig. 1, the fuel circuit includes a fertile blanket to improve breeding and a bubbling system to extract non-soluble fission products. The fuel

salt is circulated out of the core via the pumps through the heat exchangers where the heat generated is removed from the fuel salt and transferred to the intermediate circuit.

This system’s evolution during transient situations such as reactivity insertion and load following depends strongly on the neutronics and thermal hydraulics coupling due to the heat motion and the delayed neutron precursor circulation. The neutronics impacts the thermal hydraulics through the distribution of the power produced and of the precursor creations. The thermal hydraulics has feedback effects through the distributions of the delayed neutron sources and of the temperature in the core.

The Transient Fission Matrix (TFM) approach has initially been developed to model the neutronics of this kind of reactor. As discussed in Section 2, this TFM approach is designed to reproduce Monte Carlo neutronic calculations with a reduced computational cost. The neutron propagation in the reactor is pre-calculated once, prior to the transient calculation, using the Serpent Monte Carlo code (Leppänen, 2015). This information is then stored in matrices

<sup>\*</sup> Corresponding author.

E-mail address: [laureau.axel@gmail.com](mailto:laureau.axel@gmail.com) (A. Laureau).

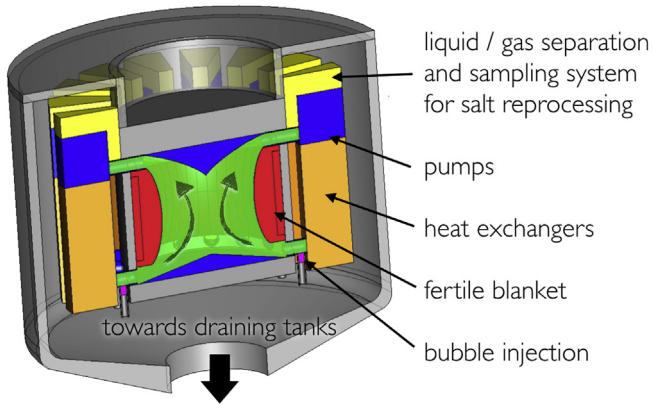


Fig. 1. MSFR fuel circuit global scheme.

for subsequent use in the kinetics calculations. An interpolation model is presented to take into account accurately the evolution of these matrices for different perturbations such as the thermal hydraulics feedback effects studied in this paper. Concerning the thermal hydraulics modeling, the complex flow pattern in the reactor can not be reproduced with sub-channel code. Thanks to the reduced fluid–solid interface in the core, the CFD (Computational Fluid Dynamics) resolution presented in Section 3 can be used for this reactor with a reasonable execution time. These two resolutions are finally coupled (Section 4) to obtain a solution of the reactor at steady state (Section 5) and to study transient scenarios (Section 6).

## 2. Neutronics modeling: Transient Fission Matrix

This section presents a brief introduction of the elements of TFM approach used in the current work, including the neutron kinetics equations solved during the coupling to the thermal hydraulics. This approach and its validation on different nuclear systems such as the Flattop experiment are detailed in Laureau et al. (2015) and Laureau (2015). Note that Section 2.5 is dedicated to the presentation of a new interpolation model adapted to the MSFR specificities: a fast spectrum reactor with an homogeneous fuel.

### 2.1. Fission matrix introduction

Fission matrices are usually employed to accelerate the source convergence in Monte Carlo neutronics codes (Carney et al., 2014; Dufek and Gudowski, 2009) or to estimate the different modes of the neutron source distribution (Carney et al., 2012).

The information contained in fission matrices is the transport of neutrons during one generation from each neutron emission-position  $j$  in the reactor to all its fission-positions  $i$ . Using a spatially discretized reactor, the emission and production positions  $i$  and  $j$  are associated to cells (or volume elements). This quantity can be directly estimated using a Monte Carlo neutronics calculation; the fission neutron production in cell  $i$  produced by a neutron created in cell  $j$  is scored in line  $i$  and column  $j$  of the fission matrix. This neutron propagation is represented in Fig. 2, the generation of the fission matrices pre-calculates and condenses the neutron propagation, and can be used a posteriori to propagate any source neutron distribution in the core.

The objective of this approach is to perform transient calculations, so that an innovative temporal aspect is added to the fission matrix approach.

### 2.2. TFM additional operators

From the usual fission matrices, additional operators have been added to develop the TFM approach. The first kind of operators are defined to take into account the distinct behavior between prompt and delayed neutrons. Different matrices are then calculated,  $\underline{G}_{\chi_x v_x}$ , where  $\chi_x$  represents the prompt or delayed emission spectrum  $\chi_p$  or  $\chi_d$ , and  $v_x$  represents the prompt or delayed production of neutrons  $v_p$  or  $v_d$ . The second kind of operators concerns the kinetic aspect: the  $\underline{T}_{\chi_p v_p}$  matrix represents the average time response from cell  $j$  to cell  $i$  associated to the prompt neutron production  $\underline{G}_{\chi_p v_p}$ .

This approach has been implemented in a modified version of the Serpent code. For each fission neutron source created in the core during a critical calculation, this neutron has an attribute corresponding to the cell number  $j$  of its birth, and another attribute indicating if this neutron is a delayed neutron. Then, at each interaction in all the cells  $i$  during the neutron transport, the probability of creating a fission neutron, prompt or delayed, is scored. The neutron lifetime weighted by the production of fission neutrons is also scored. Finally, the spatially discretized operators  $\underline{G}_{\chi_p v_p}$ ,  $\underline{G}_{\chi_d v_d}$ ,  $\underline{G}_{\chi_d v_p}$ ,  $\underline{G}_{\chi_p v_d}$  and  $\underline{T}_{\chi_p v_p}$  are estimated in one calculation using these  $j$  to  $i$  estimators.

### 2.3. Kinetic parameter calculations

The effective generation time and the effective fraction of delayed neutrons can be deduced from the properties of the generated matrices (Laureau et al., 2015). The kinetic calculations with the TFM approach presented in this paper are using the effective fission to fission time, estimated by combining the data of the fission matrix  $\underline{G}_{\chi_p v_p}$  and of the time propagation matrix  $\underline{T}_{\chi_p v_p}$ . The calculation of this effective parameter is detailed in this section.

This quantity requires an estimation of the equilibrium source neutron distribution and of the importance map. The eigenvector of  $\underline{G}_{\chi_p v_p}$  corresponds to the equilibrium prompt neutron sources  $\mathbf{N}_p$  in the reactor, its propagation through the fission matrix corresponds to a dilatation of the prompt multiplication factor:  $\underline{G}_{\chi_p v_p} \mathbf{N}_p = k_p \mathbf{N}_p$ . The transposed fission matrix corresponds to the backward transport of the neutron, the probability that a neutron created in  $j$  comes from a previous history stated in  $i$ . The associated eigenvector  $\mathbf{N}_p^*$  is the importance map of the neutrons, it represents the proportion of neutrons coming from each position.

Finally, using  $\underline{G}_{\chi_p v_p} \cdot \underline{T}_{\chi_p v_p}$  the element by element multiplication matrix, the effective fission to fission time  $l_{eff}$  can be calculated using Eq. (1). This equation consists in a local time response weighted by the local neutron production to obtain the global time response. Both numerator and denominator are adjoint weighted by the importance map to obtain the effective value. It corresponds to the effective prompt lifetime  $l_{eff}$  since non-fission reactions have a zero-importance and the importance of fission events is the importance of the produced neutrons.

$$l_{eff} = \frac{\mathbf{N}_p^* \left( \underline{G}_{\chi_p v_p} \cdot \underline{T}_{\chi_p v_p} \right) \mathbf{N}_p}{\mathbf{N}_p^* \underline{G}_{\chi_p v_p} \mathbf{N}_p} \quad (1)$$

### 2.4. Neutron kinetics equations

The kinetics equations use the effective prompt lifetime  $l_{eff}$  calculated using  $\underline{T}_{\chi_p v_p}$  discussed in Section 2.3 dealing with the kinetic

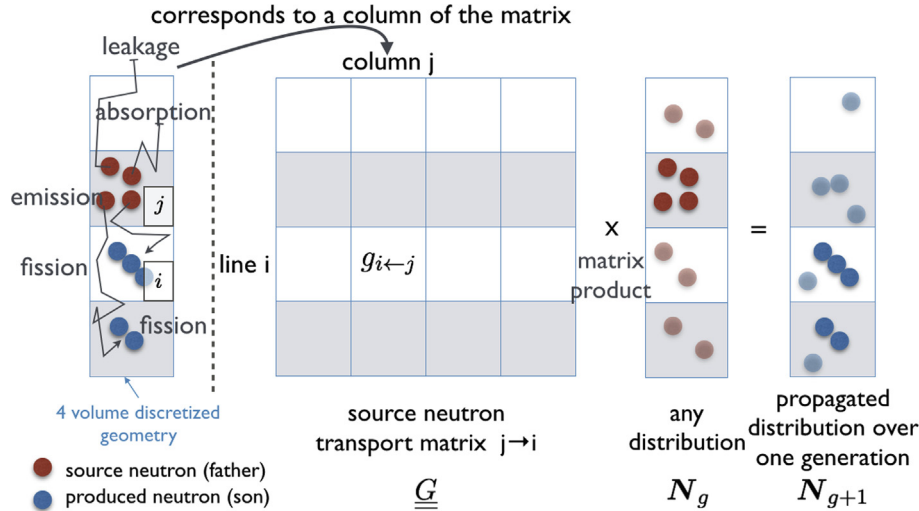


**Fig. 2.** Representation of the fission matrix element  $ij$ : neutron production in volume  $i$  induced by an incoming source neutron injected in  $j$ , and neutron propagation over one generation.

parameter calculations. Henceforth, the neutron vector  $\mathbf{N}$  is a function of time:  $\mathbf{N}(t)$ . Similarly, the fission matrices are written  $\underline{G}_{\lambda_x v_x}(t)$ , these matrices being interpolated on the fly during the calculation. A specific model presented in Section 2.5 is used to take into account the effect of the local temperature distribution on the reactivity feedback.

These equations are balanced equations. During  $dt$ ,  $\mathbf{N}(t) \frac{dt}{l_{eff}}$  prompt neutrons disappear, creating  $\underline{G}_{\lambda_p v_p}(t) \mathbf{N}(t) \frac{dt}{l_{eff}}$  new prompt neutrons, and also  $\underline{G}_{\lambda_d v_d}(t) \mathbf{N}(t) \frac{dt}{l_{eff}}$  new precursors. In the same time  $\sum_f \lambda_f \mathbf{P}_f(t) dt$  precursors disappear, generating  $\underline{G}_{\lambda_d v_d}(t) \sum_f \lambda_f \mathbf{P}_f(t) dt$  new prompt neutrons and  $\underline{G}_{\lambda_d v_d}(t) \sum_f \lambda_f \mathbf{P}_f(t) dt$  new precursors.

Finally, the kinetics equations of the prompt neutrons and of the precursors of each family  $f$  are the following:

$$\frac{d\mathbf{N}(t)}{dt} = \underline{G}_{\lambda_p v_p}(t) \mathbf{N}(t) \frac{1}{l_{eff}} + \underline{G}_{\lambda_d v_d}(t) \sum_f \lambda_f \mathbf{P}_f(t) - \frac{1}{l_{eff}} \mathbf{N}(t) \quad (2)$$

$$\frac{d\mathbf{P}_f(t)}{dt} = \frac{\beta_f}{\beta_0} \left[ \underline{G}_{\lambda_p v_p}(t) \mathbf{N}(t) \frac{1}{l_{eff}} + \underline{G}_{\lambda_d v_d}(t) \sum_f \lambda_f \mathbf{P}_f(t) \right] - \lambda_f \mathbf{P}_f(t) \quad (3)$$

We have validated this approach on effective parameter calculations and prompt neutron time dependent propagation, using the Flattop and Jezebel experiments (Laureau et al., 2015). A dedicated benchmark for liquid fuel reactors has also been realized to test time dependent aspects including precursor related phenomena (Laureau, 2015).

## 2.5. Fission matrix interpolation

### 2.5.1. Interpolation presentation

The fission matrices evolve during transient calculations because the reactor itself evolves. Different parameters such as the temperature studied in this paper can impact the neutron propagation and thus the fission matrices. The objective of this TFM approach is to avoid resorting to new Monte Carlo calculations during transient calculations. An interpolation model of the matrices has been developed for this purpose and is described below (Laureau, 2015).

This interpolation assumes that the variation of the system response during one neutron generation is negligible. For the MSFR, the system studied in this article, the effective neutron

lifetime is around  $1 \mu\text{s}$ , much less than the characteristic time of the thermal hydraulics. The approximation is thus acceptable. We consider two temperature related contributions to the variation of the matrices: the first one is associated to the fuel salt density with a linear contribution, and the other one is due to the Doppler effect with a logarithmic contribution. Three different sets of matrices are finally calculated: one for the reference state, one with a modified fuel density, and one with modified fuel cross sections. These matrices are obtained for an homogeneous variation of the Doppler/density distribution. The purpose of this section is to answer the following question: *how can we interpolate a heterogeneous temperature distribution?* Then local Doppler/density variations could be taken into account.

Note that in the TFM approach, two pieces of information are available: the temperature at the neutron birth position  $j$  and the temperature at the fission position  $i$ . The first will be called *begin*, and the other *end*. The interpolation model is based on these raw information elements.

Fig. 3 presents the neutron propagation over one generation (top) and at equilibrium (bottom) on a test case, a 1D reactor of 200 cm with the MSFR fuel salt composition. In the test case discussed here the temperature distribution comprises three different zones: 900 K on the left (50 cm), 1200 K in the middle (100 cm) and 1000 K on the right (50 cm). A neutron pulse is released near the first temperature split (at 55 cm).

Three situations are illustrated in this figure, they correspond to the two pieces of raw information (*begin* and *end*) and to the interpolation model discussed here (called “rebalanced”). The *begin* and *end* curves represent the neutron propagation with a uniform temperature distribution. These results are presented together with the reference solution (red) calculated with the Serpent code using the real discretized temperature distribution. The interpolated matrices aim at reproducing this reference result, but without new Monte Carlo calculations.

The matrices used for the interpolation are computed using a reference temperature of 900 K and a density/Doppler variation corresponding to 1200 K. The first raw information available (*begin*) is the amount of produced neutrons propagated using an interpolation based on the temperature of the neutron emission position. For example, with  $g_{i←j}$  the element of line  $i$  – column  $j$  of any matrix  $\underline{G}_{\lambda_x v_x}$ , the interpolated value is estimated using the temperature  $T_j$  of the departure cell  $j$ :

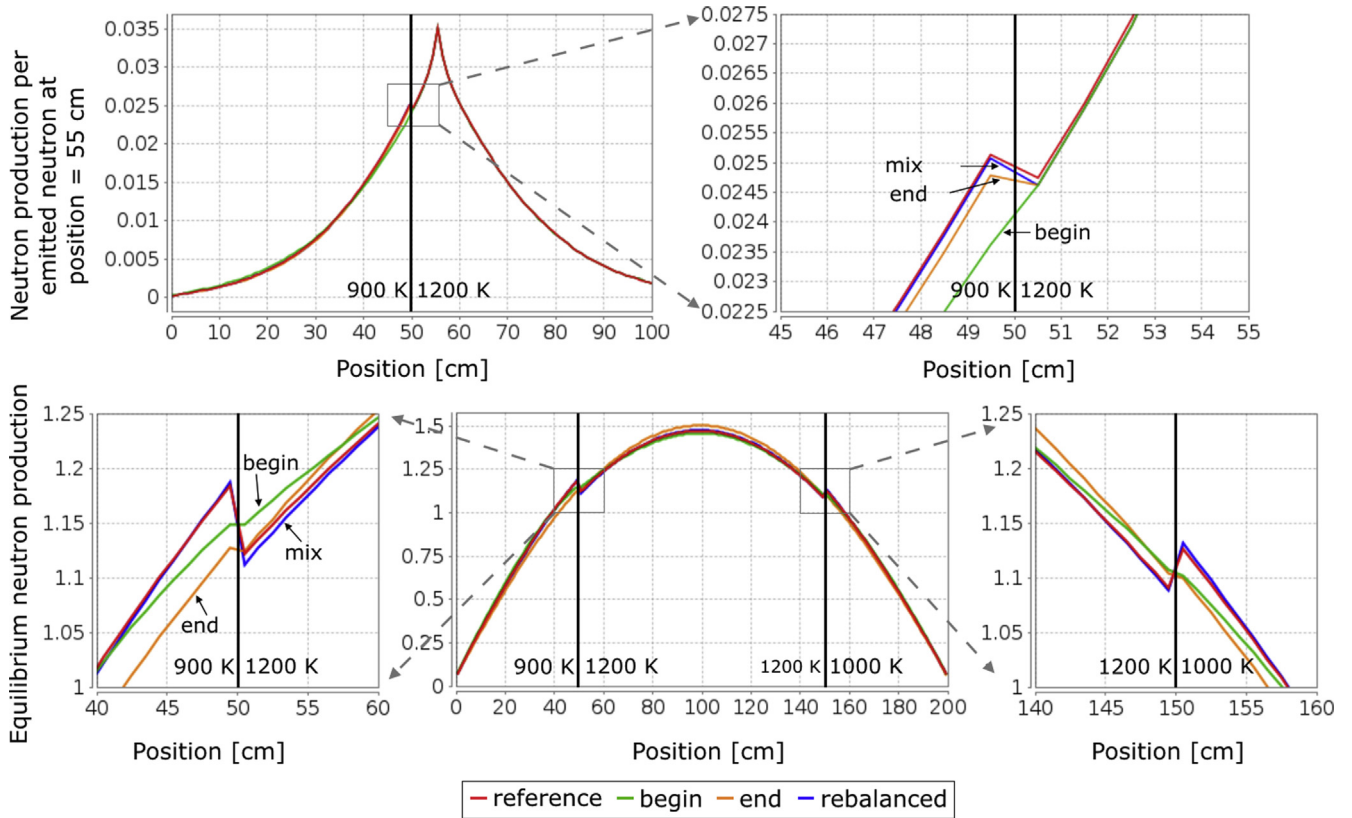


**Fig. 3.** Distribution of the produced neutrons over one generation due to a neutron emission at 55 cm (top left) with a zoom on the discontinuity (top right), and equilibrium distribution (bottom) for a temperature distribution of 900 K for pos < 50 cm, 1200 K for 50 cm < pos < 150 cm, and 1000 K for pos > 150 cm.

$$g_{i-j}^{begin} = g_{i-j}(T_j) \quad (4)$$

Similarly, with the second raw information available (*end*), the interpolated value uses the temperature  $T_i$  of the generated fission position  $i$ :

$$g_{i-j}^{end} = g_{i-j}(T_i) \quad (5)$$

As we can see in Fig. 3, the neutron propagation over one generation (top) is not properly reproduced with the *begin* information (green curve): the temperature variation is not correctly taken into account. As previously mentioned, the *end* raw information (orange curve) takes into account the correct arrival temperature. However on the equilibrium distribution (bottom), even if the *begin* information does not provide an accurate distribution near the temperature discontinuity, the value at a distance from the heterogeneity is correctly reproduced. On the contrary the *end* information seems to provide poor results at equilibrium. Indeed, even if it is supposed to be better since it takes into account the local temperature where the fission occurs, the conservation of the absorptions is not respected.

If we create the absorption matrix  $\underline{A}$  with the general term  $a_{i-j}$  corresponding to the neutron absorption distribution instead of the neutron production by fission, the sum of the absorptions in the reactor using the information *begin*  $\sum_i a_{i-j}^{begin}$  is coherent since all the terms of the column use the same temperature  $T_j$  to perform the interpolation. On the other hand,  $\sum_i a_{i-j}^{end}$  uses different temperatures  $T_i$  (*end*) for the interpolation for an emitted neutron in  $j$  (*begin*): the absorption rate is not conserved. We write  $lack_j = \sum_i a_{i-j}^{begin} - \sum_i a_{i-j}^{end}$ , the lack of absorption for each position of emission  $j$ . Finally, the *rebalanced* interpolation model combines these two pieces of raw information with the following equation:

$$a_{i-j}^{rebalanced} = a_{i-j}^{end} + lack_j \frac{|T_j - T_i| a_{i-j}^{end}}{\sum_i |T_j - T_i| a_{i-j}^{end}} \quad (6)$$

In this way, the total absorption per neutron emitted is conserved. The global neutron distribution shape is based on the *end* information, but with a renormalization linked to the *begin* information adjusting locally the shape where the temperature has evolved using  $|T_j - T_i|$ . The same correction is applied to the fission matrices, but still based on the absorptions since the fission amount is not supposed to be conserved as opposed to the absorptions:

$$g_{i-j}^{rebalanced} = g_{i-j}^{end} + lack_j \frac{|T_j - T_i| g_{i-j}^{end}}{\sum_i |T_j - T_i| a_{i-j}^{end}} \quad (7)$$

The matrix set created by this method provides the best results as seen in Fig. 3 (blue curve). Another test of this model is the estimation of the variation of the multiplication factor  $k$  compared to a direct Monte Carlo calculation, presented in Table 1.

The results obtained with the *rebalanced* interpolation model are good, with a discrepancy of only 4%. Observe that other models can be developed. For other kinds of reactors, specific developments could be required, the rebalanced model being accurate and adequate for the present application and being used in the calculations presented in Section 5. An application to the impact of control rods in pressurized water reactors shows that a very good prediction of the flux redistribution in the core and of the multiplication factor can be obtained using this interpolation model (Laureau, 2015).

A validation of this interpolation model is presented in Section 4.4 on a representative case of the MSFR with a complex

**Table 1**Estimation of the variation of  $k$  by the interpolation model compared to the homogeneous reference case at a temperature of 900 K.

Method	Reference	Begin	End	Rebalanced
Variation (pcm)	$-1174 \pm 2$	$-1358 \pm 2$	$-1354 \pm 2$	$-1222 \pm 2$
Discrepancy	–	+15.6%	+15.4%	+4.1%

temperature and density distributions and the precursor transport phenomena.

### 3. Thermal hydraulics modeling

The system studied here is the liquid fuel MSFR reactor, characterized by a flowing liquid fuel which also serves as coolant for heat transport from the core to the heat exchangers. The thermal hydraulics modeling is essential in such a system, to deal with the heat extraction and the motion of the delayed neutron precursors. Because the flow pattern in the core is complex, one dimensional flow models do not provide enough accuracy.

Different strategies can be followed to solve the Navier–Stokes equations modeling the thermal hydraulics phenomena broadly referred to as CFD codes. The one adopted here is called the Reynolds-Averaged Navier–Stokes (RANS) approach. It consists in solving the time-average value of the different parameters while modeling the fluctuations with different turbulence models. The high frequency turbulences are cut off and a good estimation of the hydraulics pattern is obtained at a reasonable cost. The equations solved are detailed below.

The fluid is considered to be incompressible ( $\rho = \rho_0$ ), so that the mass equation can be simplified as:

$$\nabla \cdot (\bar{\mathbf{u}}) = 0 \quad (8)$$

where  $\bar{\mathbf{u}}$  is the average of the velocity vector  $\mathbf{u}$  and  $\nabla \cdot ()$  the divergence operator.

The momentum equation is:

$$\begin{aligned} \frac{\partial(\bar{\mathbf{u}})}{\partial t} + \nabla \cdot (\bar{\mathbf{u}} \otimes \bar{\mathbf{u}}) = & -\frac{1}{\rho_0} \nabla \left( \bar{p} + \frac{2}{3} k \right) + \nabla \\ & \cdot \left( \nu_{eff} \left( \frac{1}{2} (\nabla(\bar{\mathbf{u}}) + \nabla(\bar{\mathbf{u}})^t) - \frac{2}{3} \nabla \cdot \bar{\mathbf{u}} \underline{\underline{d}} \right) \right) \\ & + \mathbf{g} (1 + \beta_{buoyancy} (\bar{T} - T_0)) \end{aligned} \quad (9)$$

where  $\bar{p}$  is the average pressure. The kinetic turbulent energy  $k$  and the turbulent viscosity  $\nu_{eff}$  are both calculated by the turbulence model (Shih et al., 1995), the k-epsilon realizable turbulence model being used in this study. The last term corresponds to the Boussinesq approximation expressing the buoyancy force as:  $\mathbf{g} (1 + \beta_{buoyancy} (\bar{T} - T_0))$ , where  $\beta_{buoyancy}$  is the fluid thermal expansion coefficient,  $\bar{T}$  the fuel average temperature and  $\mathbf{g}$  the gravitational acceleration.

Finally, the energy balance equation is:

$$\frac{\partial \bar{T}}{\partial t} + \nabla \cdot (\bar{T} \bar{\mathbf{u}}) = \kappa_{eff} \Delta(\bar{T}) + S_{external} \quad (10)$$

where  $\kappa_{eff}$  is the effective diffusivity coefficient, which accounts for the turbulent diffusivity. Observe the external source term  $S_{external}$  which corresponds to the power released by the fissions; it is calculated by the neutronics module.

### 4. Numerical implementation & coupling strategy

The main two codes used in this study are Serpent for the neutronics, and OpenFOAM for the thermal hydraulics. Serpent is a Monte Carlo neutronics calculation code (Leppänen, 2015), and OpenFOAM is an open source CFD calculation code (Jasak et al.,

2007). In both cases, specific procedures have been included directly in the source code to implement the TFM approach.

#### 4.1. Neutronics module

The neutronics module is split in two parts, the calculation of the discretized operators  $G_{\lambda_k, \nu_k}$ , and the numerical integration of the kinetics equations.

The transient fission matrices are computed prior to the transient calculation using Serpent. Serpent estimates the fission matrices in a single calculation using a tetrahedral mesh (3600 cells, Fig. 4-right) imported from OpenFOAM. The variations of the operator with the density and the Doppler are determined via two other distinct calculations. For each calculation, 2.5 billions of neutron are simulated in order to obtain a statistical error on the reactivity smaller than to 1 pcm.

The integration of Eqs. (2) and (3) is directly implemented in the thermal hydraulics source code since no more Monte Carlo calculations are required once the matrices have been generated. The temperature field calculated by the thermal hydraulics is used to interpolate the matrices during the transient.

#### 4.2. Thermal hydraulics module

The thermal hydraulics solution is obtained using the OpenFOAM CFD calculation code. The utilisation of this code for the MSFR study and the optimisation of the numerical parameters have been validated in the frame of a dedicated benchmark (Merle-Lucotte et al., 2014)

A finer mesh is required to perform the CFD calculation (87,000 cells, Fig. 4-left) than for TFM (Fig. 4-right). A specific optimization of the CFD mesh is required for the thermal hydraulics to capture the flow pattern in the inlet of the core with the detachment of the boundary layer (Rouch et al., 2014) The cross-mapping of the different fields between the meshes is performed by OpenFOAM using internal libraries based on standard finite volume mapping techniques. In order to limit the computation complexity using a symmetry boundary condition, the simulations are performed on 1/16 of the reactor, corresponding to one recirculation loop. The pumps and the heat exchangers visible on the right of the geometry in Fig. 4 are modeled as a porous media.

The power density field in the reactor is a source term in the energy Eq. (10). In this study, it is considered as proportional to the neutrons produced by fission to avoid calculating the energy matrix: the energy release associated to the neutron transport from cell  $j$  to cell  $i$ . The whole fission energy is considered as locally released at the fission position. The delayed neutron precursor transport is also performed by OpenFOAM, using the source term calculated by the neutronics.

#### 4.3. Coupling approach

The algorithm usually employed in OpenFOAM to obtain the implicit convergence of all the resolved parameters consists in iterative calculations of all the physics during one time step. These iterations are called “outer” iterations. In this way, during transient calculations, the solution obtained satisfies all the solved equations.

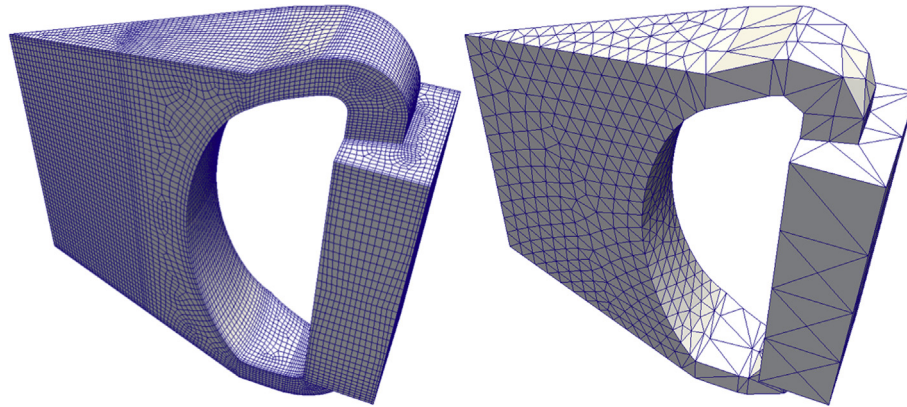


Fig. 4. MSFR meshes for the thermal hydraulics (left) and the neutronics (right).

The same approach is used for this coupling including the neutronics module in these outer iterations, this module being directly implemented in OpenFOAM. However, the time steps used for the neutronics ( $\sim \mu s$ ) are much smaller than those of thermal hydraulics ( $\sim ms$ ). During one thermal hydraulics time step, many neutronics time steps are performed (Fig. 5). The temperature field calculated by the thermal hydraulics is interpolated during the neutronics calculation, and the energy source term or the precursor source term is inferred from the average production of the neutronics steps.

4.4. Validation of the interpolation model on a MSFR representative case

In order to check this interpolation model with a complex temperature distribution, a 2D case with a simple neutronics thermal hydraulics coupling representative of the MSFR temperature field and precursor motion has been defined (Laureau, 2015) The reference calculations are based on a direct Monte Carlo – CFD coupling performed with the Serpent and OpenFOAM codes (Aufiero, 2014).

The case geometry is a 2D square of  $2 \times 2$  meters with a reference neutronic power of 1 GW/m and a uniform surface heat extraction coefficient of  $10^6$  W/K/m<sup>2</sup>. Different configurations have been defined in this study with an increasing complexity, from a first level with some elementary neutronic and thermal hydraulics tests, to a more complex level of static and dynamic couplings between these two physics. The configuration presented here to illustrate this validation process includes a fuel motion due to the buoyancy force implied by the fuel expansion of  $2.10^{-4}$  K<sup>-1</sup>. The velocity, temperature, and some of the precursors fields calculated are presented in Fig. 6. The temperature distribution is impacted by the fuel motion that, with the natural convection, implies a shift of the maximum temperature to the top of the

geometry. The temperature range of 900 up to 1350 K is representative of the possible temperature variation in the MSFR during accident scenarios. Note that the precursors are linked to the fuel, so that their distribution is strongly impacted if their lifetime is large enough (around some seconds).

Fig. 7 presents a comparison of the results obtained with TFM and direct reference Monte Carlo calculations. Two elements are compared here: the reactivity variation according to the imposed power level (left), and the effective fraction of delayed neutrons  $\beta_{eff}$  (right). Concerning the reactivity variation, we can see that a very good agreement is obtained. At the maximum power of 1 GW/m, the error on the reactivity variation is around only 2%. Concerning  $\beta_{eff}$  comparisons, an excellent agreement is also obtained. Note that the value of this parameter depends on the amount of precursors decaying in the areas with a reduced neutronic importance. For this reason, when the power increases, the temperature increases, and finally the velocity increases too due to the buoyancy force. Then if the power is equal to zero, the  $\beta_{eff}$  is equal to the usual “static”  $\beta_{eff}$ , and when to power increases the  $\beta_{eff}$  is logically reduced. As we can see, the  $\beta_{eff}$  calculated using the TFM approach is compatible with the reference values obtained with the direct Serpent–OpenFOAM calculations.

To conclude, a very good agreement is obtained between TFM and a direct Monte Carlo calculation on this case representative of MSFR transient calculations, illustrating the capability of the matrix interpolation to model the MSFR physics on the fly in such situations.

5. Reference MSFR system

5.1. MSFR configuration

The characteristics of the reference MSFR configuration at nominal power are summarized in Table 2.

The fuel salt thermodynamical properties used in this study are given in Table 3. They are assumed to be constant.

5.2. Steady state solution

Obtaining the steady state solution is a preliminary step since it is used to initialize transient calculations. This image of the reactor is solution of both neutronics and thermal hydraulics equations.

Various parameters are constrained: the power level and the average fuel temperature are fixed to reference values (here respectively at 3 GWth and 975 K for the nominal power solution), and the delayed neutron source is normalized (here using  $\sum_j \lambda_j P_j$ ). The neutron population and distribution, the temperature and

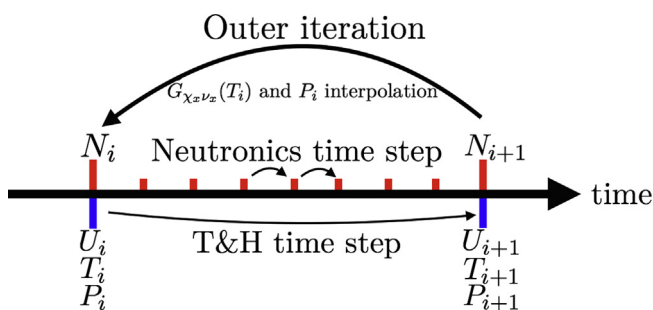
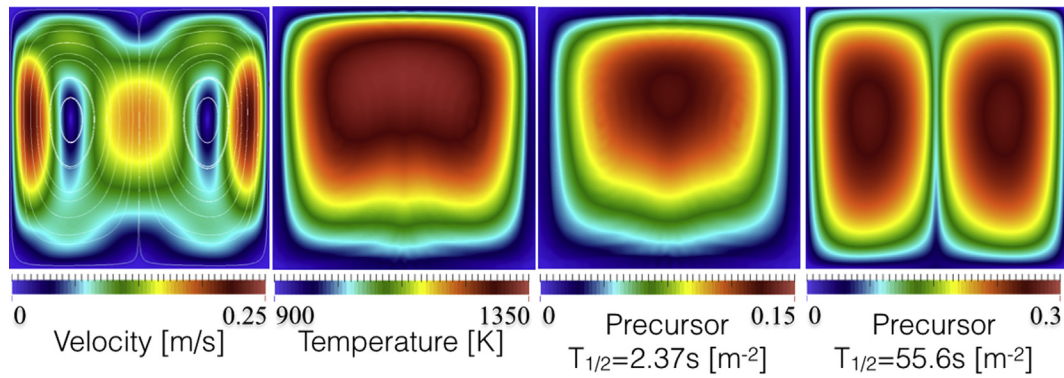
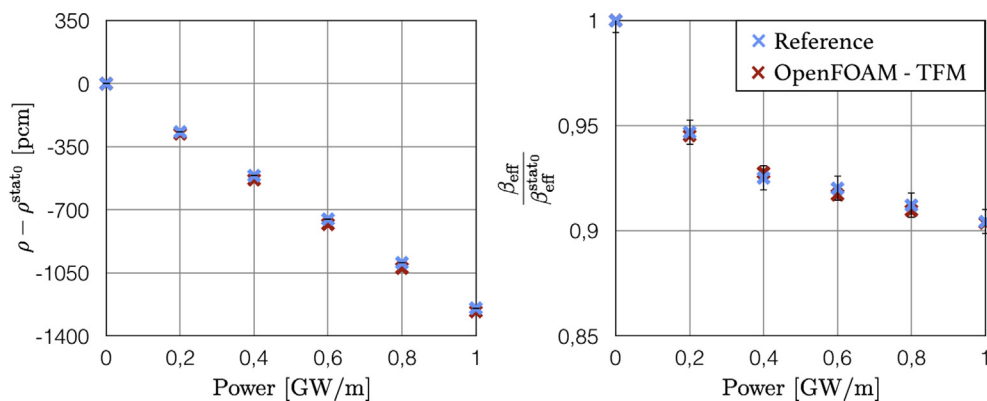


Fig. 5. Numerical scheme of the TFM–OpenFOAM coupling.



**Fig. 6.** Results of the coupled calculation for the 1 GW/m configuration in natural convection. Equilibrium distribution of the velocity (with stream lines), temperature, and precursors for two different decay constants.



**Fig. 7.** Reactivity variation (left) and normalised effective fraction of delayed neutrons (right) calculated with TFM (red) and direct Monte Carlo with the statistical uncertainty (blue) for different imposed powers (For interpretation of the references to colour in this figure legend, the reader is referred to the web version of this article.).

**Table 2**  
Characteristics of the reference MSFR at nominal power.

Parameter	Value
Thermal power	3000 MWth
Mean fuel salt temperature	975 K
Mean fuel salt heating in the core	100 K
Fuel salt composition	LiF-ThF <sub>4</sub> - <sup>233</sup> U (77.5-20-2.5 mol%)
Total fuel salt volume	18 m <sup>3</sup>
Total fuel salt cycle in the fuel circuit	4 s
Total feedback coefficient	-8 pcm/K

**Table 3**  
Fuel salt thermodynamical properties at 975 K.

Parameter	Symbol	Unit	Value
Kinematic viscosity	$\nu$	m <sup>2</sup> /s	2.46 10 <sup>-6</sup>
Dilatation factor	$\beta_{buoyancy}$	K <sup>-1</sup>	2.14 10 <sup>-4</sup>
Prandtl number	Pr	-	16
Turbulent Pr	Pr <sub>turb</sub>	-	0.85
Density	$\rho$	kg/m <sup>3</sup>	4125
Specific heat capacity	C <sub>p</sub>	J/kg/K	1594

precursor distributions, and the velocity field are then resolved and a unique solution is obtained. Note that the temperature of the intermediate fluid in the heat exchangers is iteratively adjusted to obtain a power extraction corresponding to the power produced in the core. The steady state solution obtained at nominal power is displayed in Fig. 8.

The velocity distribution (Fig. 8 top-left and stream lines at the bottom) illustrates the complex flow pattern in the reactor, requiring a CFD calculation to capture the vortex and the recirculation at the core inlet. The maximum power production (middle-left) calculated with the TFM model in OpenFOAM is logically located in the middle of the core, and the difference between the neutronics discretization and the thermal hydraulics discretization can be observed. The global temperature increase is also displayed (middle-right), with a limited effect of the recirculation thanks to the low power level in this area. A hotspot may be noticed at the top of the reactor due to the low velocity. Finally, the precursor distribution (right) is very inhomogeneous. The maximum value obtained at the top of the reactor corresponds to the precursor families with a short lifetime. The families with a long time constant circulate in the whole fuel circuit, inducing a non-negligible production of precursors in the recirculation loops and thus an effective fraction of delayed neutrons  $\beta_{eff}$  reduced to 124 pcm while the physical fraction is 310 pcm.

## 6. Transient calculations

Different MSFR transient studies have been performed, corresponding to normal and incidental situations. In this paper we first discuss the reactor's load following capabilities with different cases calculated to illustrate how the reactor can be driven by the heat extraction. Incidental scenarios are then presented, such as reactivity insertions and overcooling transients with a large range of initial power and of intermediate fluid thermal inertia.

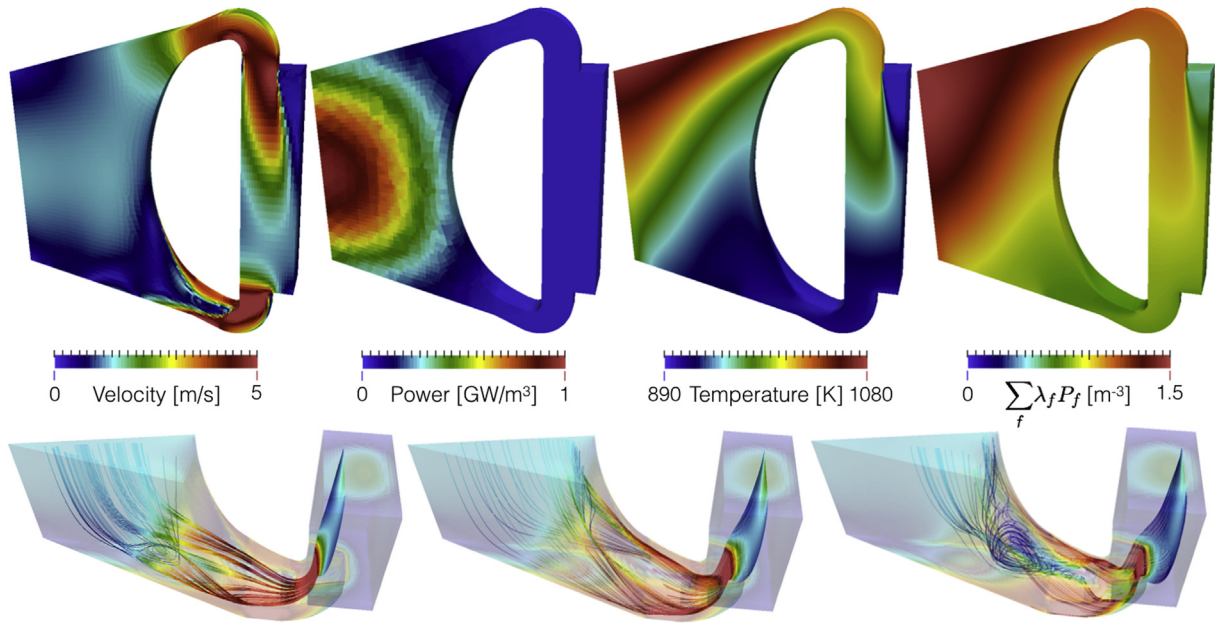


Fig. 8. Top-left: distribution of the velocity module; bottom: stream lines with the local velocity module; top-middle-left: power distribution; top-middle-right: fuel temperature distribution; top-right: delayed neutron distribution normalized to 1.

6.1. Load following transient

The load following capacity is an important aspect of electricity production in countries with a large share of electro-nuclear generation. A maximum 5% per minute of power variation (Lokhov, 2011) is reachable with pressurized water reactors. Other electricity generators such as gas-fueled generators allow a 20% per minute variation. The limitation incurred by nuclear reactors is thus due to the way the heat is generated and not to the turbines. The purpose of this section is to study the MSFR capability to perform load followings from the neutronics and thermal hydraulics point of view, independently of other issues such as materials and thermomechanical considerations.

Fig. 9 presents a 33% variation of the nominal power in 60 s driven by a variation of the intermediate fluid temperature. During all the following transient calculations, three parameters are monitored as represented in Fig. 9:

- The prompt criticality margin,  $k_p - 1$  (left). Even if the (prompt) multiplication factor is not directly used during the calculation, the eigenvalue of  $G_{\chi_p, v_p}$  provides a good evaluation of the prompt criticality margin.
- The produced power (middle) in solid line, and the extracted power in dashed line, the latter being calculated on the fly using the local distribution of temperature in the heat exchanger.
- The mean temperature of the fuel salt. This value is obtained by averaging the temperature on the whole fuel circuit: core, heat exchangers and pipes.

A reactivity increase is observed for the 3 to 2 GW case (red curve). No active regulation of the reactivity is performed: the cooling and the negative thermal feedbacks lead to a spontaneous reactivity increase, and thus the neutronic power in the core follows the extracted power with a delay of only one second (due to the fuel motion). Finally, the slow equilibration of  $k_p - 1$  is linked to the time constant of the precursor equilibration.

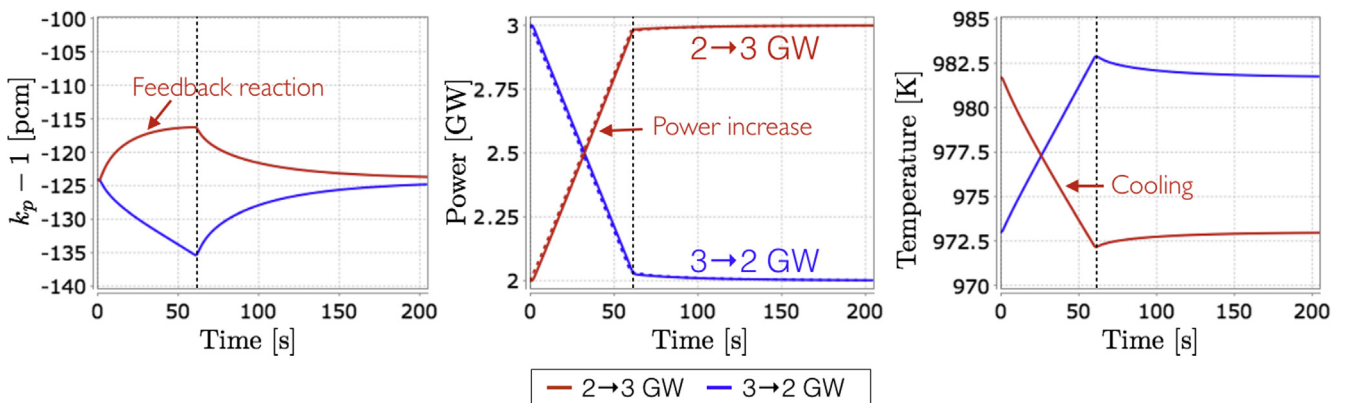


Fig. 9. Evolution of the margin to prompt criticality ( $k_p - 1$ ), of the power, and of the mean fuel salt temperature for a load following in 1 min from 2 to 3 GW (red curves) and from 3 to 2 GW (blue curves) (For interpretation of the references to colour in this figure legend, the reader is referred to the web version of this article.)

The second case is a load following from 3 to 2 GW (blue curve). A similar behavior with a reversed amplitude is observed with a decrease of the reactivity.

These cases highlight the good behavior of the reactor on load following transients regarding the neutron kinetic and the thermal hydraulics aspects of the fuel circuit. Control rods are not required to drive the reactor. Further studies relative to the heat exchangers, together with the intermediate and energy conversion circuits, are still required to assess the actual reactor ability to achieve such transients.

## 6.2. Overcooling incident

The second kind of transient we discuss in this paper is the overcooling incident. This scenario can lead to a prompt critical situation. The objective here is to study the reactor behavior and the sensitivity to the initial operating conditions in this situation.

In order to consider a bounding case, a low initial power level and a very short time constant of the power variation in the heat exchangers have been selected. Thus, the feedback effects are delayed: even a power increase of many orders of magnitude has a limited impact on the temperature. Two systematic studies are discussed here: an instantaneous power variation (not realistic but upper bound) for different initial powers; and a low initial power fixed at 1 kW with different power time constants. Note that such a low initial power remains a realistic scenario, for example during the reactor start-up procedure.

### 6.2.1. Parametric study on the initial power level

In Fig. 10, we show instantaneous overcooling transient calculation results for different situations. The overcooling is obtained via an instantaneous modification of the intermediate fluid tempera-

ture in the heat exchangers. The initial power level at the beginning of the transient ranges from 1 kW to 2 GW.

Fig. 11 illustrates, for the case with a 100 MW initial power, the initial temperature distribution  $T(t=0)$  (left) and its variation  $T(t) - T(0)$  at various times during the transient.

In the case of an initial power of 2 GW, the reactivity insertion is not fast enough to lead to a prompt critical situation. During the first moments, the temperature decrease induces a reactivity increase and then the produced power increases. After 2 s, the power reaches a level high enough to stabilize the reactivity.

Even an initial power of 100 MW is large enough to avoid a prompt critical behavior. The reactivity margin is reduced to 15 pcm but the feedback effects are fast enough to counterbalance the power increase of 30 times the initial power. As we can see in Fig. 11, the fuel salt is immediately cooled down in the heat exchangers. The cooled salt enters the core cavity whose beginning is observed at that time. At the 1.5 and 2 s time steps, the temperature increase in the reactor due to the power variation can be observed. Between 3 and 5 s, the temperature increases at the reactor inlet due to the propagation of the fuel salt heated by the power burst at 1.5 s. This reinjection of the heated salt in the core induces the reactivity decrease observed at 4 s (Fig. 10-left).

With an initial power less than 10 MW, the reactor reaches a prompt critical behavior. The power increases faster and the maximum power is 3.3 GW for the case starting from 10 MW. For an initial power of 1 kW, the maximum power reached is 20 GW. In both cases, the fuel temperature increase during the prompt critical situation is small, equal respectively to only 0.1 and 2 K, even if the energy is released over a very short duration ( $\sim 0.02$  s). The fuel salt dilatation is then very fast.

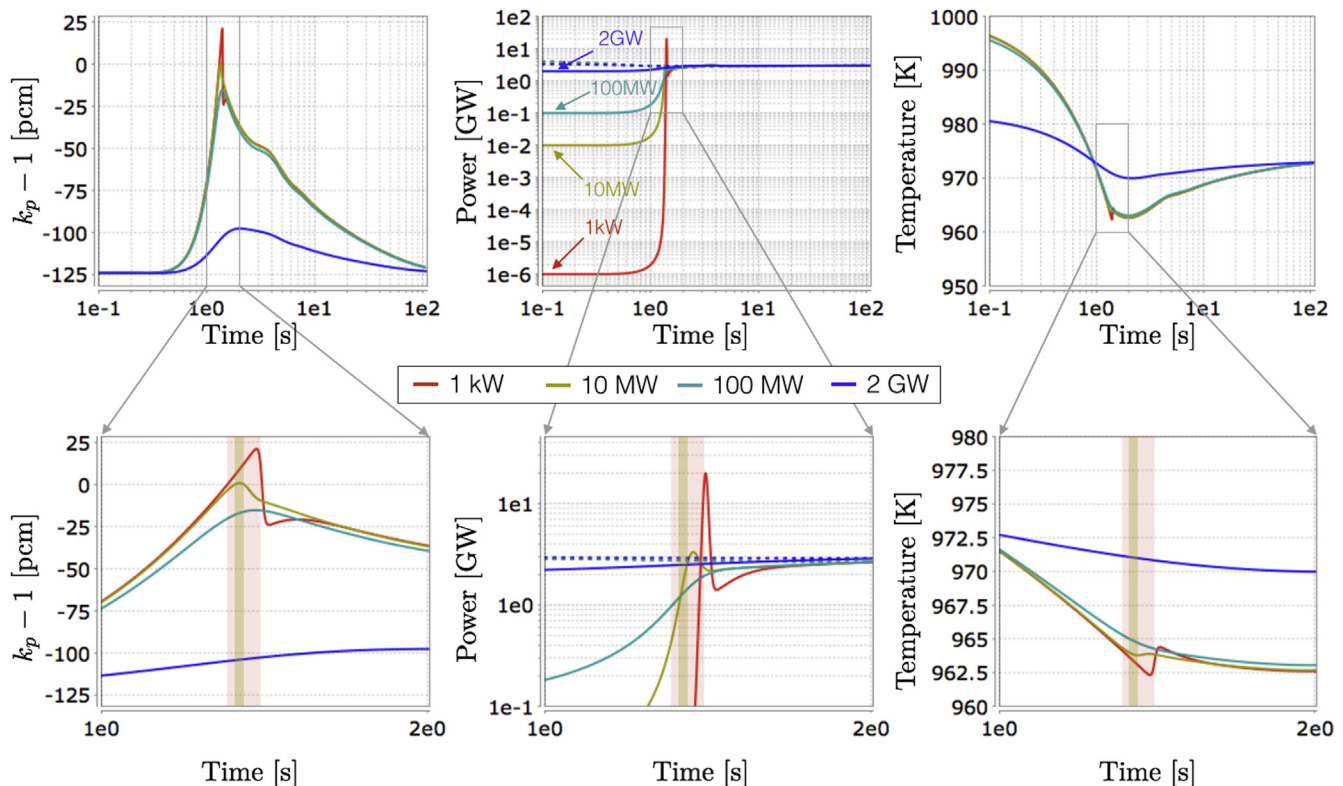


Fig. 10. Evolution of  $k_p - 1$ , of the power, and of the mean fuel salt temperature for instantaneous overcooling transient cases from 2 GW, 100 MW, 10 MW and 1 kW up to 3 GW (For interpretation of the references to colour in this figure legend, the reader is referred to the web version of this article.).

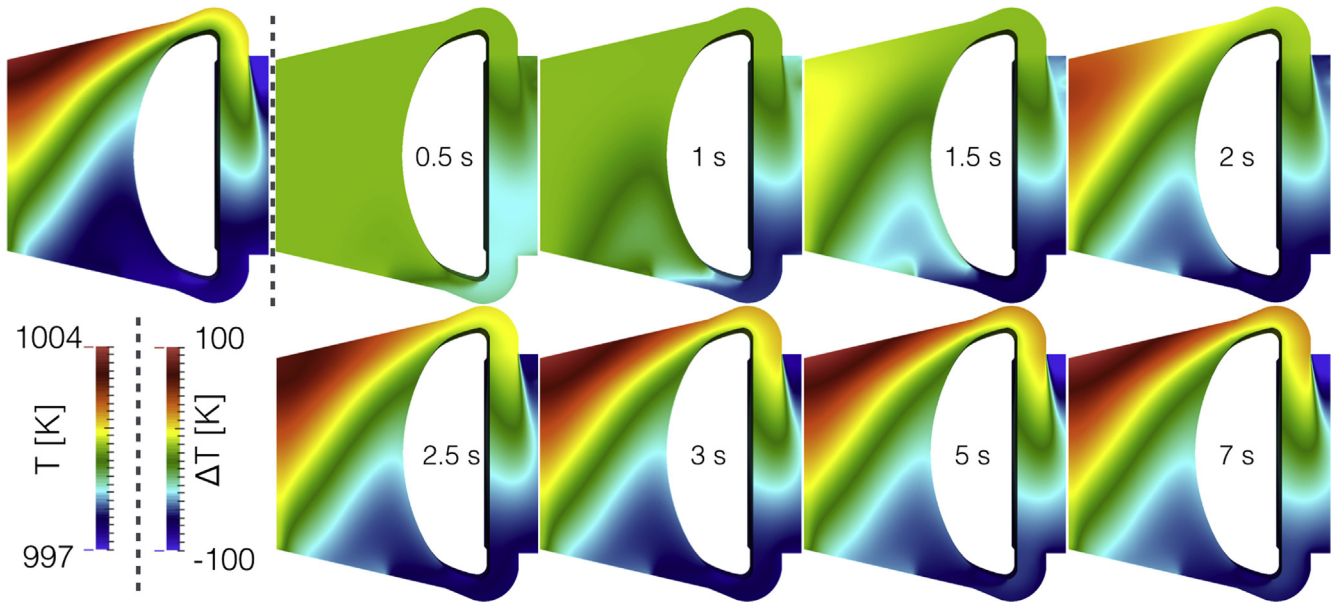


Fig. 11. Temperature distribution at  $t = 0$  (left), and its variation  $T(t) - T(0)$  at different time steps of the 100 MW-3 GW overcooling transient.

6.2.2. Parametric study on the time constant of the power variation

The system inertia (heat exchanger, pumps...) is such that the extracted power variation can not be instantaneous. Indeed, assuming for example that the pumps are fitted with flywheels, the time constant can range from a few seconds to some minutes.

Fig. 12 presents a parametric study, based on a 1 kW up to 3 GW overcooling transient, with a linear variation of the intermediate fluid temperature in 1 up to 128 s (compared to the previous case of 0 s).

The time constant of the overcooling transient has a huge impact on the maximum power reached. With a time constant of

16 s, the reactor is still slightly prompt critical, but the power excursion is limited to 1.5 GW and the variation of the temperature to 0.3 K in ~0.1 s. For time constants larger than 32 s, the prompt critical situation is avoided.

The study demonstrates how the system inertia can contribute to mitigating the reactor perturbation via an increased time constant. Thanks to the feedbacks, even an overcooling at 1 kW does not lead to prompt criticality for a time constant larger than 30 s. Note that the fuel salt temperature variation is not large even for a time constant of 16 s where the prompt critical regime is reached. However, the impact of such a fast temperature variation

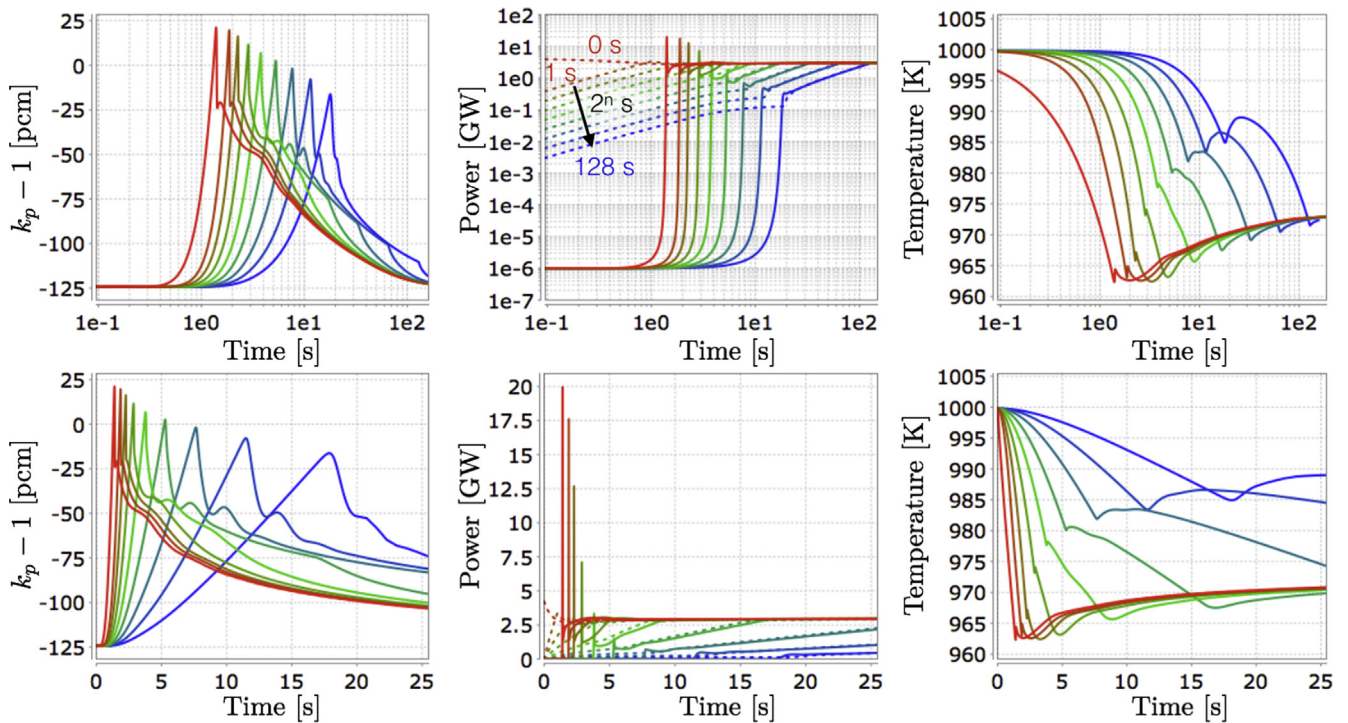


Fig. 12. Evolution of  $k_p - 1$ , of the power, and of the mean fuel salt temperature for a 1 kW up to 3 GW overcooling transient with a time constant between 0 and 128 s.

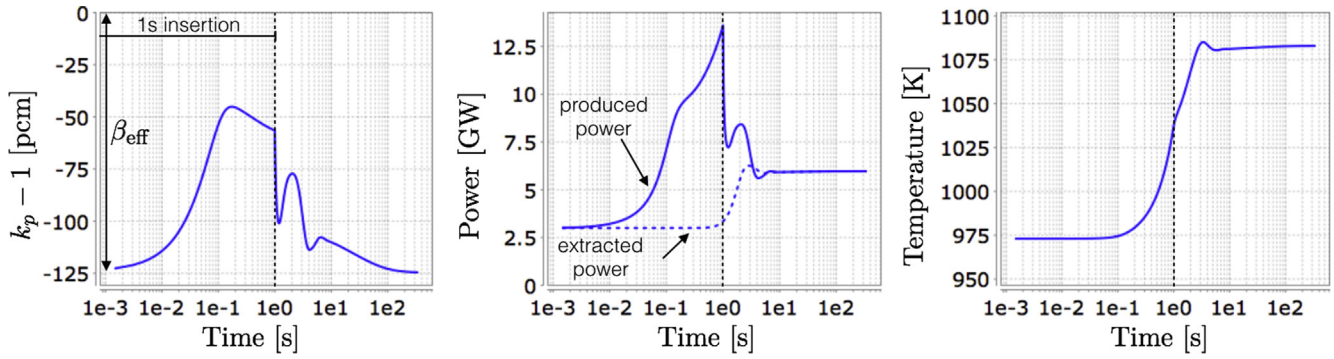


Fig. 13. Evolution of  $k_p - 1$ , of the produced and extracted power, and of the mean fuel salt temperature for an insertion of 1000 pcm in 1 s.

and thus of the dilatation of the liquid fuel on the whole circuit has to be evaluated, especially in regard to mechanical constraints.

### 6.3. Reactivity insertion accident

Such transients are studied with an overall variation of the reactivity so as to evaluate the reactor behavior without defining a specific scenario. The reactivity insertion is simulated by multiplying the fission matrices by a constant, thus modifying the eigenvalue directly.

#### 6.3.1. Bounding case: 1000 pcm in 1 s

The section focuses on a reactivity insertion of 1000 pcm in 1 s (see Fig. 13). This case corresponds to the maximum reactivity margins available in the MSFR (Institut de Radioprotection et de Sûreté Nucléaire, 2015) with a time constant characteristic of the salt transport between the recirculation loops and the core.

Fig. 14 presents the initial fuel salt temperature distribution  $T(t=0)$  (top-left) and its variation  $\Delta T(t) = T(t) - T(0)$  during the transient. The second line presents the normalized power and its variation in order to show the flux redistribution in the reactor induced by the temperature evolution.

The analysis of this transient can be split in three time intervals: before 0.1 s, between 0.1 and 1 s, and after 1 s. At the beginning of the transient calculation ( $t < 0.1$  s), the prompt multiplication factor increases as a result of the reactivity insertion. The variation

induces an increase of the produced power. However, the temperature does not evolve in such a small time interval.

After 0.1 s, the power reaches 7.5 GW and starts to impact the temperature. The reactivity increase stops thanks to the consecutive feedback effect. Since the reactivity insertion is constant, one would expect the temperature to increase at a constant rate providing exact corresponding feedback, and thus the power change rate should be constant up to 1 s. However, as Fig. 14 shows, the fuel motion is not negligible during the first second and the hot salt moves from the middle to the top of the core. This motion induces a progressive power increase up to 13.5 GW at 1 s.

Finally, after the energy release of the first second, the power stabilizes to a new level which corresponds to the new power extraction in the heat exchangers (dashed line) in accordance with the fuel salt temperature increase. An oscillation can be noted around 3 s due to the fuel circulation between the core and the heat exchangers, the outgoing heated salt being replaced by cold salt at the core inlet.

A large fuel temperature variation is incurred during this transient. A 350 K increase at about 1.5 s (Fig. 14-top) implies a power redistribution at the bottom of the core (Fig. 14-bottom).

This study demonstrates the very good reaction of this reactor to a large reactivity insertion for the time interval typically required to propagate a perturbation from the heat exchanger to the core with the fuel motion.

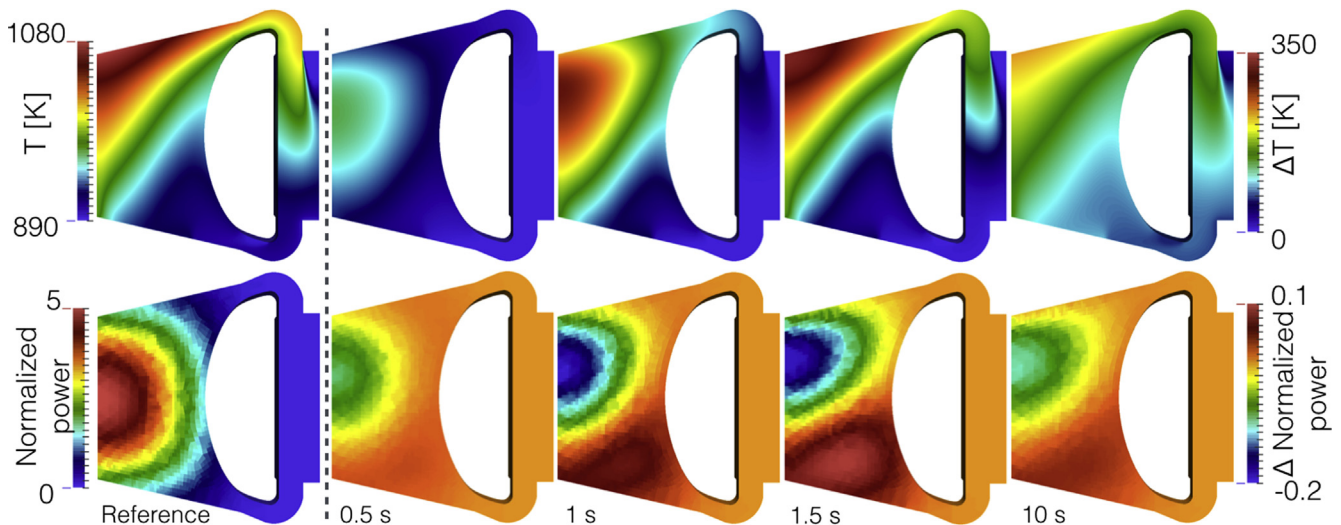


Fig. 14. Top: Temperature distribution at  $t = 0$  s (left), and its variation  $\Delta T(t) = T(t) - T(0)$  at different time steps of the transient; bottom: normalized power distribution at  $t = 0$  s (left), and its variation at different time steps of the transient.

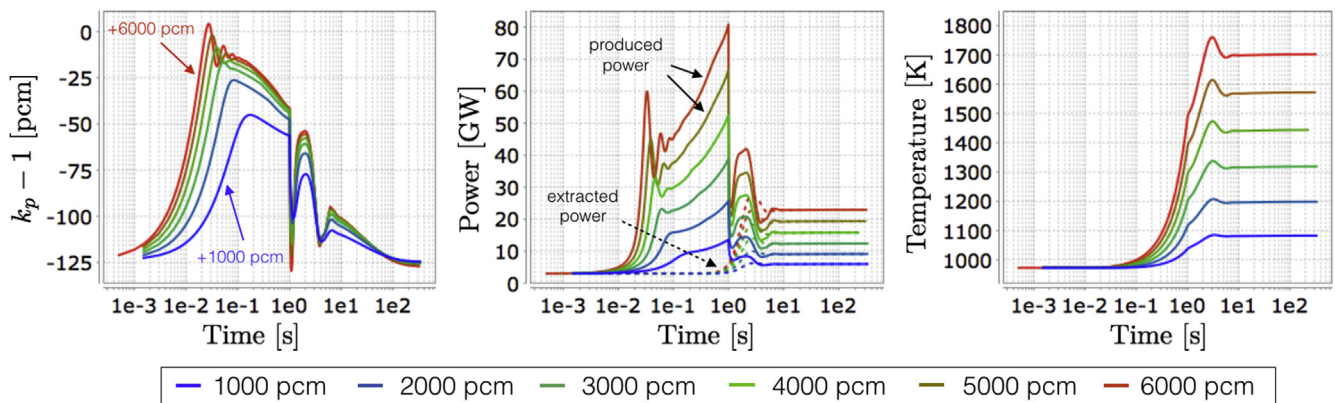


Fig. 15. Evolution of  $k_p - 1$ , of the produced and extracted power, and of the mean fuel salt temperature for reactivity insertions of 1000 pcm to 6000 pcm in 1 s.

### 6.3.2. Parametric insertion in 1 s

The purpose of this second study is to estimate the reactivity margin to prompt criticality, and to understand the reactor behavior during a violent transient. This parametric study does not rest on a realistic situation since the MSFR does not have such a large reactivity reserve (Brovchenko, 2013). Fig. 15 presents reactivity insertions from 1000 up to 6000 pcm in 1 s.

The only case leading to a prompt critical situation ( $k_p > 1$ ) is the insertion of 6000 pcm. However, the transition between the prompt subcritical and critical situation is not sharp: oscillations during the first step of the transient ( $t < 0.1$  s) appear at 4000 pcm in 1 s. These oscillations are induced by the competition between the reactivity insertion rate and the energy released growth rate.

The maximum average temperature reached during the transient only slightly overshoots the equilibrium value (+60 K for an increase of 700 K) thanks to the good reactor behavior. However, the final temperature can not be sustained by the materials for a long time period, an active or passive system would have to drain the reactor within a few minutes to avoid damage.

## 7. Conclusions

The neutronic TFM approach coupled to the thermal hydraulics code OpenFOAM proves to be an efficient tool to investigate coupled phenomena in nuclear systems. It can deal with precursor motion effects on the chain reaction thanks to the TFM approach and with a complex flow pattern via the CFD calculation. The interpolation model presented here can evaluate perturbed fission matrices in order to take into account the flux redistribution and the reactivity variation due, for example, to an evolution of the temperature distribution in the reactor. Comparisons with reference calculations demonstrate how closely the interpolated solution approaches the reference calculation. Moreover, thanks to its short computation time, the interpolation can be done for each time step of the transient.

Based on this code development, normal and incidental transient scenarios of the MSFR system have been studied. The maximum reactivity insertion of 1000 pcm in 1 s can be sustained by the reactor thanks to the feedback effect, the power level adjusting efficiently the fuel salt temperature to keep the reactor subcritical. The load following capability of this concept has also been demonstrated regarding the core behavior, confirming that control rods are not required to drive this reactor. The overcooling incident has been identified as a possible initiator to a prompt critical situation, even if the flywheel impact on the intermediate circuit can maintain the reactor subcritical thanks to the inertia introduced.

These studies evidence the MSFR's good behavior during these situations.

Future work will focus on the analysis of various transient situations for the MSFR reactor safety and optimization studies, and on the application of this coupling tool on different reactors such as PWRs.

## Acknowledgments

The authors wish to thank the NEEDS (Nucléaire: Energie, Environnement, Déchets, Société) French programs, the IN2P3 department of the National Centre for Scientific Research (CNRS), Grenoble Institute of Technology, and the European program EVOL (Evaluation and Viability of Liquid Fuel Fast Reactor System) of FP7 for their support. We are also thankful to Elizabeth Huffer for her help during the proofreading of this paper.

## References

- Allibert, M., Aufiero, M., Brovchenko, M., Delpech, S., Ghetta, V., Heuer, D., Laureau, A., Merle-Lucotte, E., 2016. Chapter X – Molten Salt Fast Reactors, Handbook of Generation IV Nuclear Reactors. Woodhead Publishing Series in Energy.
- Aufiero, M., 2014. Development of advanced simulation tools for circulating fuel nuclear reactors. Politecnico di Milano, Italie. Ph.D. thesis.
- Brovchenko, M., 2013. Études préliminaires de sûreté du réacteur à sels fondus MSFR. Université de Grenoble, France. Ph.D. thesis.
- Brovchenko, M., Heuer, D., Merle-Lucotte, E., Allibert, M., Ghetta, V., Laureau, A., Rubiolo, P., 2013. Design-related studies for the preliminary safety assessment of the molten salt fast reactor. Nucl. Sci. Eng. 175 (3), 329–339.
- Carney, S., Brown, F., Kiedrowski, B., Martin, W., 2012. Fission matrix capability for mcnp monte carlo. Trans. Am. Nucl. Soc. 107, 494.
- Carney, S., Brown, F., Kiedrowski, B., Martin, W., 2014. Theory and applications of the fission matrix method for continuous-energy monte carlo. Ann. Nucl. Energy 73, 423–431.
- Dufek, J., Gudowski, W., 2009. Fission matrix based monte carlo criticality calculations. Ann. Nucl. Energy 36 (8), 1270–1275.
- Heuer, D., Merle-Lucotte, E., Allibert, M., Brovchenko, M., Ghetta, V., Rubiolo, P., 2014. Towards the thorium fuel cycle with molten salt fast reactors. Ann. Nucl. Energy 64, 421–429.
- Institut de Radioprotection et de Sûreté Nucléaire, Review of Generation IV Nuclear Energy Systems, Expert Report, avril 2015.
- Jasak, H., Jemcov, A., Tukovic, Z., 2007. OpenFOAM: A C++ Library for complex physics simulations. International workshop on coupled methods in numerical dynamics, vol. 1000, pp. 1–20.
- Laureau, A., 2015. Développement de modèles neutroniques pour le couplage thermohydraulique du MSFR et le calcul de paramètres cinétiques effectifs. Université Grenoble Alpes, France. Ph.D. thesis.
- Laureau, A., Aufiero, M., Rubiolo, P., Merle-Lucotte, E., Heuer, D., 2015. Transient fission matrix: kinetic calculation and kinetic parameters  $\beta_{eff}$  and  $z_{eff}$  calculation. Ann. Nucl. Energy 85, 1035–1044.
- Leppänen, J., Pusa, M., Viitanen, T., Valtavirta, V., Kalliaisena, T., 2015. The Serpent Monte Carlo code: Status, development and applications in 2013. Ann. Nucl. Energy 82, 142–150.
- Lokhov, A., 2011. Technical and economic aspects of load following with nuclear power plants. Nuclear Development Division, OECD NEA.

- Merle-Lucotte, E., Rouch, H., Alcaro, F., Allibert, M., Aufero, A., Cammi, A., Dulla, S., Feynberg, O., Frima, L., Geoffroy, O., Ghetta, V., Heuer, D., Ignatiev, V., Kloosterman, J.-L., Lathouwers, D., Laureau, A., Luzzi, L., Merk, B., Ravetto, P., Rineiski, A., Rubiolo, P., Rui, L., Szieberth, M., Wang, S., Yamaji, B., 2014. Optimization of the pre-conceptual design of the MSFR. Tech. rep., EVOL European FP7 project, Work-Package WP2, Deliverable D2.2.
- Rouch, H., Geoffroy, O., Rubiolo, P., Laureau, A., Brovchenko, M., Heuer, D., Merle-Lucotte, E., 2014. Preliminary thermal-hydraulic core design of the Molten Salt Fast Reactor. *MSFR. Ann. Nucl. Energy* 64, 449–456.
- Shih, T.-H., Liou, W.W., Shabbir, A., Yang, Z., Zhu, J., 1995. A new  $k-\epsilon$  eddy viscosity model for high reynolds number turbulent flows. *Comput. Fluids* 24 (3), 227–238.